International Journal of Heat and Mass Transfer 52 (2009) 4711–4721

Contents lists available at ScienceDirect

International Journal of Heat and Mass Transfer

journal homepage: www.elsevier.com/locate/ijhmt

Predictions of turbulent flow and heat transfer in gas–droplets flow downstream of a sudden pipe expansion

V.I. Terekhov *, M.A. Pakhomov

Kutateladze Institute of Thermophysics, Lab. of Thermal and Gas Dynamics, Russian Academy of Sciences, Siberian Branch, 1, Acad. Lavrent'ev Avenue, Novosibirsk 630090, Russia

ARTICLE INFO

Article history:
Received 12 February 2009
Received in revised form 5 May 2009
Accepted 16 June 2009
Available online 22 July 2009

Keywords:
Gas–droplets turbulent flow
Evaporation
Euler/Euler two-fluid model
Separated flow

ABSTRACT

Droplets-laden turbulent flow downstream of a sudden pipe expansion has been investigated by using Euler/Euler two-fluid model for the gaseous and dispersed phases. Significant increase of heat transfer in separated flow at the adding of evaporating droplets has been demonstrated (more than 2 times compare with one-phase flow at the value of mass concentration of droplets $M_{L1} \leqslant 0.05$). Addition of dispersed phase to the turbulent gas flow results in insignificant increase of the reattachment length. Low-inertia droplets ($d_1 \leqslant 50$ μm) are well entrained into the circulation flow and present over the whole pipe section. Large particles ($d_1 \approx 100$ μm) go through the shear layer not getting into the detached area. Comparison with experimental data on separated gas–droplets flows behind the plane backward-facing step has been carried out.

© 2009 Elsevier Ltd. All rights reserved.

1. Introduction

The detached flows in a sudden expansion pipe frequently encountered in technical applications [1–5]. The detachment affects momentum, heat, and mass transfer processes to a large extent determines the turbulent flow structure. Knowledge of the turbulent flow field and heat transfer in sudden expansion flows is important from both theoretical and practical points of view. Sudden pipe expansions are used to stabilize flame in combustion chambers. Other numerous applications of sudden pipe expansions imply their use as step diffusers or as heat transfer intensifiers in ducted flows. Thus such flows have become a subject of many extensive studies. Studies one-phase separated flows past a backward-facing step or downstream of the sudden expansion were reported in many publications, which are reviewed [6–13].

On the basis of these works we have come to the conclusions stated further on. At the distance approximately (20–25)H after detachment the flow gets specificity of the developed flow in the pipe, although, final stabilization occurs much lower along the flow. Here H is the step height. In the plane channel it happens at the distance $x/H \approx 50$. Values of fluctuations and Reynolds stress have complex character of distribution both along the pipe length and along its radius with specific maximum in the shear layer. Maximum values of axial fluctuations intensity are $\langle u'^2\rangle \leqslant 0.2U_1$, where U_1 is the flow velocity before detachment. Radial fluctuations are less than axial ones and are equal to $\langle v'^2\rangle \leqslant 0.15U_1$. At this, at the distance $20H$ the value of axial fluctuations is higher than that of the radial ones that serves an extra proof of non-stabilized and non-isotropic flowing in this area. According to the data [11] the value of velocity fluctuations in transversal direction is $\langle w'^2\rangle \approx \langle v'^2\rangle$. Whereas, for detachment behind the plane backward-facing step the measured values are $\langle w'^2\rangle \approx (\langle u'^2\rangle + \langle v'^2\rangle)/2$.

Heat transfer rate in the area of reattachment of detached flow is much higher than at intact flow. The value of maximum coefficient of heat transfer is proportionate to the Reynolds number in the degree of 2/3. Minimum of heat transfer is approximately at the distance between the step height and the detachment point of the flow, that is explained by the present area of secondary recirculation of the flow, which effect on heat transfer is mentioned in a number of works [8,11,12]. The value of average velocity and intensity of turbulent fluctuations in this area is much less than in the zone of detached flow. All above mentioned facts prove great complexity of the modeling of the impulse and heat transfer processes in detached one-phase flows.

Two-phase separated flows have been found in many technical applications. The effect of solid/liquid particles on transport process in the gas phase becomes more pronounced with increasing size and concentration of the particles. Detailed information concerning the turbulent flow, the velocities and temperatures of the phases, and the distribution of particles over the pipe cross-section is an important matter for optimization of evaporation/combustion processes. Two-phase separated flows were investigated [14–26]. These authors showed that, light particles are entrained in the circulating flow, whereas heavy particles escape trapping in the separation zone by traversing the shear flow region. In the wall zone

* Corresponding author. Tel.:+7 383 330 67 36; fax: +7 383 330 84 80.
E-mail address: terekhov@itp.nsc.ru (V.I. Terekhov).

0017-9310/$ - see front matter © 2009 Elsevier Ltd. All rights reserved.
doi:10.1016/j.ijheatmasstransfer.2009.06.018

Nomenclature

C_D drag coefficient of evaporating droplets
D_{Lij} tensor turbulent diffusion of particles (m^2/s)
d droplet diameter (m)
$ER = (R_2/R_1)^2$ or $ER = (h_1 + H)/h_1$ expansion ratio
g_u, g_{ut} coefficients of entrainment of particles into large-eddy velocity and temperature fluctuation motion of gas phase
h channel height (m)
H step height (m)
J mass flux of vapor from the surface of evaporating droplets (kg/(m s))
k turbulent kinetic energy (m^2/s^2)
K_A; K_V mass concentration of air and vapor in binary vapor–air mixture
K_{VS} mass concentration of vapor at the drop surface an evaporating corresponding to saturation parameters at the drop temperature, T_L
L turbulent length scale (m)
M_L mass fraction of droplets
$\overline{R}$ absolute gas constant (J/(mol K))
$\langle uv\rangle = -\nu_T \frac{\partial U}{\partial r}$, $\langle u_L v_L\rangle$ turbulent stresses in gas and dispersed phases (m^2/s^2)
$\langle u^2\rangle$, $\langle v^2\rangle$ root-mean-square velocity fluctuations in axial and radial directions (m^2/s^2)
x_R reattachment length (m)
$y_\lambda = y/\sqrt{\nu k/\varepsilon}$ Taylor microscale (m)
Pr Prandtl number
$\mathrm{Re}_L = \rho d\sqrt{(U-U_L)^2 + (V-V_L)^2}\mu$ Reynolds number of disperse phase
Stk = τ/τ_f mean-flow Stokes number
Tu turbulence intensity in the flow

Greek symbols
ε dissipation of the turbulent kinetic energy (m^2/s^3)
Φ volume concentration of particles
$I^E = 2\langle u^2\rangle^{1/2}\Omega^L$ turbulent scale of gas phase (s)
$\Theta = (T - T_W)/(T_1 - T_W)$ temperature profile
$\Omega^\varepsilon = (15\nu/\varepsilon)^{1/2}$ time microscale (s)
Ω^E Eulerian time macroscale (s)
Ω^L Lagrangian time macroscale (s)
$\Omega^{\varepsilon L}$ time of particle interaction with the intense vortices (s)
$\tau = \rho_P d^2/(18\mu W)$ particle relaxation time (s)
$\tau_f = 5H/U_1$ turbulent time scale in the mean motion (s)
$\tau_\Theta = C_{pL}\rho_L d^2/(12\lambda Y)$ particle thermal relaxation time (s)

Subscripts
0 parameter at the axis of the pipe
1 parameter before separation
2 parameter after separation
A air
L dispersed phase
P particle
T turbulent parameter
V vapor

Symbol
$\langle\ \rangle$ ensemble average

Acronym
LRN low-Reynolds number
PDA phase Doppler anemometer
PDF probability density function
TKE turbulent kinetic energy

dispersed impurities are accumulated (preferential concentration). It is noted that papers [14,16–18,21,23,25] were provided for the backward-facing step flow geometry, and works [15,16,18–20,22,24]-for the flow downstream of pipe sudden expansion.

Zaichik et al. [16,18] were among the first workers who used the Eulerian/Eulerian approach in computations of gas-particles separated flows. Results obtained by these authors fairly well agree with experimental data obtained for two-phase flows downstream of a backward-facing step and sudden pipe expansion. The authors have shown that with the growth of the particle size profile of disperse phase velocity changes, becoming more uniform, and the degree of particles entrainment into recirculation gas motion decreases. Present interphase averaged and fluctuation interaction strongly affects the processes of gas and disperse particles mixing. It should be noted that in the mentioned studies gas flows laden with solid particles were examined without heat transfer between channel wall and two-phase flow.

Turbulent flow of gas and solid particles mixture with application of the method of large eddy simulation (LES) for the gas phase and Lagrangian trajectory method for the particles was studied in the work [23] for the case of non-steady 2D flows. The model does not take into account two-way coupling effect of disperse phase on transport process and gas phase turbulence. Numerical modeling of the flow behind backward-facing step has been carried out for the experimental conditions of the work [21]. Particles dispersion depending on Stokes number Stk = τ/τ_f, where $\tau = \rho_L d^2/(18\ \mu W)$-relaxation time of the particles considering deviation from the Stokes law of flowing $W = (1 + \mathrm{Re}_L^{2/3}/6)$; $\mathrm{Re}_L = (\vec{U} - \vec{U}_L)d/\nu$-Reynolds number of the particle; τ_f-time scale of the turbulence in averaged motion. It has been shown that accumulation of particles in the detached zone occurs at small Stokes numbers (small size of the particles), at large Stokes numbers disperse phase does not interact with turbulent gas eddies.

Only several studies in which turbulent flow with evaporating water droplets behind a backward-facing step were addressed by [17,24,25]. In [20,28] measured the velocities and turbulent kinetic energies of the two phases, the dispersed phase mass flow rate, and the local heat transfer from the heated wall to the gas–droplets flow. Effect of droplets evaporation was especially pronounced behind the reattachment point of the gas–droplet flow [18]. The influence of wall temperature, gas-flow temperature, and initial flow velocity on the heat transfer augmentation was analyzed.

Analysis of the works has shown that given research is carried out in the narrow diapason of changed main thermogasodynamic parameters such as drop size and their concentration. Practically there is no data on heat transfer and structure of gas–drop flow after sudden pipe expansion. This work logically follows the work [27], dedicated to numerical modeling of gas–drop flow at present phase transfers on sudden pipe expansion.

The purpose of the present study was numerical examination the effect of key parameters of the two-phase flow, namely, the mass concentration of liquid droplets and the droplet size, on heat transfer, and to compare data obtained by the developed model with previously reported experimental and numerical results for downward turbulent two-phase flows downstream of the sudden pipe expansions. This paper logically follows the work [24], dedicated to numerical modeling of gas–droplets flow downstream of the sudden pipe expansion.

2. Problem statement

In the present paper, evolution of a gas–droplet turbulent flow in the downstream region of a sudden pipe expansion was examined. A schematic of the sudden expansion gas–droplets flow is shown in Fig. 1. The volume concentration of the dispersed phase was assumed to be low ($\Phi_1 < 10^{-4}$), and the particles were assumed to be sufficiently fine ($d_1 < 100$ μm), so that, according to [19] he effects due to inter-particle collisions could be neglected when treating hydrodynamic and heat and mass transfer processes in the two-phase flow.

All computations were performed for monodispersed gas–droplets flow. The computational domain is the pipe with the zone of sudden expansion. All calculations were performed assuming a uniform wall heat flux (q_W = const). The heat flux was $q_W = 1$ kW/m^2. The pipe surface was dry, that no liquid film from deposited droplets formed on the wall. This assumption for heated channels was allowably (see [26]). This condition is valid, if the temperature difference between the wall and the droplet is higher than 40 °C. The authors believed that the drop temperature along its radius remains constant since Bio number is $\mathrm{Bi} = \alpha_L d/\lambda_L \ll 1$.

3. Numerical model

The momentum, heat and mass transfer process in the gas and dispersed phases were studied using the Eulerian approach. This approach is based on the PDF for the coordinates, velocities and temperatures of droplets in the turbulent flow (see [27]).

3.1. Gaseous phase equations

The system of Reynolds-averaged Navier–Stokes equations for a two-phase steady-state axisymmetric flow with ignored mass forces is

$$\rho\frac{\partial U_j}{\partial x_j} = \frac{6J}{d}\Phi$$

$$\rho\frac{\partial(U_jU_i)}{\partial x_j} = -\frac{\partial(P+2k/3)}{\partial x_i} + \frac{\partial}{\partial x_j}\left[(\mu+\mu_T)\left(\frac{\partial U_i}{\partial x_j}+\frac{\partial U_j}{\partial x_i}\right)\right] - (U_i-U_{Li})\frac{\Phi}{d}\left[\frac{1}{8}C_D\rho|\vec{U}-\vec{U}_L|+J\right] + \rho_L g_u\langle u_iu_j\rangle\frac{\partial\Phi}{\partial x_j}$$

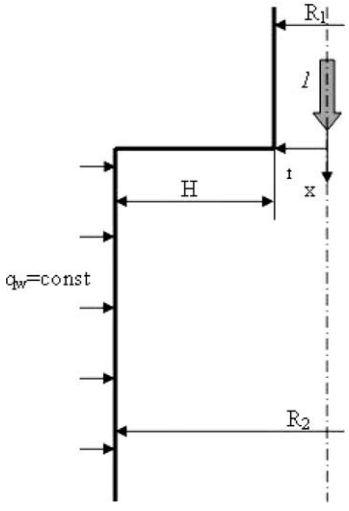

Fig. 1. The schematic of the sudden expansion gas–droplets flow. *1* – gas–droplets flow.

$$\rho\frac{\partial(U_jT)}{\partial x_j} = \frac{\partial}{\partial x_j}\left(\frac{\mu}{\mathrm{Pr}}+\frac{\mu_T}{\mathrm{Pr}_T}\right)\frac{\partial T}{\partial x_j} - \frac{6\Phi}{C_P d}[\alpha(T-T_L)+JL] + \frac{\rho D_T}{C_P}(C_{PV}-C_{PA})\left(\frac{\partial K_V}{\partial x_i}\frac{\partial T}{\partial x_i}\right) + \frac{C_{PL}\rho_L\tau g_{ut}}{C_P}\langle u_jt\rangle\frac{\partial\Phi}{\partial x_j}$$

$$\rho\frac{\partial(U_iK_V)}{\partial x_i} = \frac{\partial}{\partial x_i}\left(\frac{\mu}{\mathrm{Sc}}+\frac{\mu_T}{\mathrm{Sc}_T}\right)\frac{\partial K_V}{\partial x_i} + \frac{6J\Phi}{d}$$

$$\rho = P/(\bar{R}T). \tag{1}$$

Here, C_D is the evaporating droplets drag coefficient [29]

$$C_D = \frac{C_{DP}}{1+C_P(T-T_L)/L},$$

where C_{DP} is the drag coefficient of non-evaporating particles, which can be calculated from the relations presented by Clift et al. [28]

$$C_{DP} = \begin{cases} 24/\mathrm{Re}_L, & \mathrm{Re}_L \le 1 \\ 24/\mathrm{Re}_L(1+0.15\mathrm{Re}_L^{0.687}), & \mathrm{Re}_L > 1. \end{cases}$$

The turbulent Prandtl and Schmidt numbers were assumed constant, equal to $\mathrm{Pr}_T = \mathrm{Sc}_T = 0.85$. In addition in the work we have used correlation for calculation of turbulent Prandtl number specified in the work [29]. Difference in calculation results for the Nusselt number for one-phase flow at the use of $\mathrm{Pr}_T = 0.85$ and formula in [29] turned out to be insignificant (not more than 3%).

The turbulent Reynolds stresses and the turbulent heat and mass fluxes in the gaseous phase were determined according to the Boussinesque hypothesis; they have the form

$$\langle u_iu_j\rangle = -\nu_T\left(\frac{\partial U_i}{\partial x_j}+\frac{\partial U_j}{\partial x_i}\right)+\frac{2}{3}k\delta_{ij},\quad \langle u_jt\rangle = -\frac{\nu_T}{\mathrm{Pr}_T}\frac{\partial T}{\partial x_j},\quad \langle u_jk_V\rangle = -\frac{\nu_T}{Sc_T}\frac{\partial K_V}{\partial x_j}$$

Here, δ_{ij} is the Kronecker delta, and ν_T is the turbulent kinematic viscosity.

3.2. LRN k–$\tilde{\varepsilon}$ turbulence two-equation model

The equations for the turbulent kinetic energy k and for the dissipation rate $\tilde{\varepsilon}$ modified to the case of a two-phase flow can be written as

$$\rho\frac{\partial(U_jk)}{\partial x_j} = \frac{\partial}{\partial x_j}\left[\left(\mu+\frac{\mu_T}{\sigma_k}\right)\frac{\partial k}{\partial x_j}\right] - \frac{1}{2}\frac{\partial}{\partial x_j}\left[\mu\frac{k}{\varepsilon}\frac{\partial\tilde{\varepsilon}}{\partial x_j}\right] + \rho\Pi - \rho\varepsilon + S_k, \tag{2}$$

$$\rho\frac{\partial(U_j\tilde{\varepsilon})}{\partial x_j} = \frac{\partial}{\partial x_j}\left[\left(\mu+\frac{\mu_T}{\sigma_\varepsilon}\right)\frac{\partial\tilde{\varepsilon}}{\partial x_j}\right] + \frac{\partial}{\partial x_j}\left(\mu\frac{\tilde{\varepsilon}}{k}\frac{\partial\tilde{\varepsilon}}{\partial r}\right) + \frac{\rho\tilde{\varepsilon}}{k}(C_{\varepsilon1}f_1\Pi - C_{\varepsilon2}\tilde{\varepsilon}f_2) + S_\varepsilon, \tag{3}$$

$$\mu_T = \frac{\rho C_\mu f_\mu}{1+(\Pi/\tilde{\varepsilon}-1-A_k/\tilde{\varepsilon})/E}\frac{k^2}{\tilde{\varepsilon}}. \tag{4}$$

The constants and the damping functions were employ in the form of Hwang and Lin [30]. The adoption of the Taylor microscale in the damping functions and the inclusion of pressure diffusion terms in both the k and $\tilde{\varepsilon}$ equations were key features of this model. The designed model not only to conform with the near-wall characteristics obtained from DNS data but also to possess correct asymptotic behaviors in the vicinity of the solid wall. The performance of the model of [30] is assessed by comparison with DNS results for fully developed channel flow, with DNS results for developed Couette–Poiselle flow, and with the experiments of the 2D backward-facing step flow with heat transfer of [31]. The present model predicted correctly the skin friction and heat transfer between the wall and the air stream in the separation flow.

In (4), E is the constant in the Rotta approximation for the correlations of pressure pulsations with deformation rate (see [32]). With $\Pi/\tilde{\varepsilon} = 1$ and $A_k = 0$, expression (4) yields the classical expression

$\mu_T = \rho C_\mu f_\mu k^2/\tilde{\varepsilon}$ appearing in the turbulence model. The minimum admissible value of $E = 1$ [33]. With $E = 1$, Eq. (4) reduces to $\mu_T = \rho C_\mu f_\mu k^2/\Pi$ [16]. In the present study, with due consideration given to data reported by Zaichik et al. [16,18] the value $E = 2$ was adopted. Relation (4) results when one expands the system of implicit algebraic equations for Reynolds stresses in terms of the mean velocity gradient [16]. This modification of (4) leaves the turbulence equations unchanged. Here, the coefficient A_k stands to allow for the backward influence of particles on the shear stresses [18].

The terms S_k and S_ε characterize the additional dissipation of the gas phase turbulence due to fine evaporating droplets present in the flow and due to the non-uniform particle concentration profile; for these terms, expressions previously used by Terekhov and Pakhomov [34] were adopted.

3.3. Dispersed phase

The set of mean governing equations in the dispersed phase has the form

$$\frac{\partial U_{Lj}}{\partial x_j} = -\frac{6J\Phi}{d}$$

$$\rho_L \frac{\partial(\Phi U_{Lj} U_{Li})}{\partial x_j} + \rho_L \frac{\partial(\Phi\langle u_{Li}u_{Lj}\rangle)}{\partial x_j} = \Phi(U_i - U_{Li})\frac{\rho_L}{\tau} + \Phi\rho_L g - \frac{1}{\tau}\frac{\partial(\rho_L D_{Lij}\Phi)}{\partial x_j}$$

$$\rho_L \frac{\partial(\Phi U_j T_{Li})}{\partial x_j} + \frac{\partial}{\partial x_j}(\rho_L \Phi\langle\theta u_{Lj}\rangle) = \Phi(T_i - T_{Li})\frac{\rho_L}{\tau_\Theta} - \frac{1}{\tau_\Theta}\frac{\partial(\rho_L D^\Theta_{Lij}\Phi)}{\partial x_j} \qquad (5)$$

Here, $D_{Lij} = \tau(\langle u_{Li}u_{Lj}\rangle + g_u\langle u_i u_j\rangle)$, $D^\Theta_{Lij} = \tau_\Theta\langle u_{Lj}t_L\rangle + \tau g_{ut}\langle u_j t\rangle$ – tensors of turbulent diffusion and turbulent heat flux in dispersed phase [18]. g_u, g_{ut} – coefficients of entrainment of particles into large-eddy velocity and temperature fluctuation motion of gas phase [18].

3.4. Relations for the Reynolds stresses, temperature fluctuations and turbulent heat flux in the dispersed phase

The Reynolds stresses $\langle u_{Li}u_{Lj}\rangle$ and temperature fluctuations $\langle\theta_L^2\rangle$, and also the turbulent heat flux in dispersed phase $\langle\theta_L u_{Lj}\rangle$ were calculated using the equations by Simonin [35], and Zaichik et al. [16]. We utilized the model of [35] for Reynolds stresses, and model by Zaichik et al. [16] for temperature fluctuations and the turbulent heat flux in dispersed phase

$$\underbrace{U_{Lk}\frac{\partial\langle u_{Li}u_{Lj}\rangle}{\partial x_k}}_{I} + \underbrace{\frac{1}{\Phi}\{\frac{\partial}{\partial x_k}(\Phi\langle u_{Li}u_{Lj}u_{Lk}\rangle)\}}_{II} + \underbrace{\langle u_{Li}u_{Lk}\rangle\frac{\partial U_{Lj}}{\partial x_k} + \langle u_{Lj}u_{Lk}\rangle\frac{\partial U_{Li}}{\partial x_k}}_{III}$$
$$= \underbrace{\frac{2}{\tau}(f_u\langle u_i u_j\rangle - \langle u_{Li}u_{Lj}\rangle)}_{IV}$$

$$\underbrace{U_{Lk}\frac{\partial\langle\theta_L^2\rangle}{\partial x_k}}_{I} + \underbrace{\frac{1}{\Phi}\left\{\frac{\partial}{\partial x_k}\left(\Phi\langle u_{Lk}\theta_L^2\rangle\right)\right\}}_{II} + \underbrace{2\langle u_{Lk}\theta_L^2\rangle\frac{\partial T_L}{\partial x_k}}_{III}$$
$$= \underbrace{\frac{2}{\tau_\Theta}\left(f_\Theta\langle t^2\rangle - \langle\theta_L^2\rangle\right)}_{IV}$$
$$\times \underbrace{U_{Lk}\frac{\partial\langle\theta_L u_{Lj}\rangle}{\partial x_k}}_{I} + \underbrace{\frac{1}{\Phi}\left\{\frac{\partial}{\partial x_k}(\Phi\langle u_{Li}u_{Lk}\theta_L\rangle)\right\}}_{II} + \underbrace{\langle u_{Li}u_{Lk}\rangle\frac{\partial T_L}{\partial x_k} + \langle u_{Lk}\theta_L\rangle\frac{\partial U_{Li}}{\partial x_k}}_{III}$$
$$= \underbrace{\left(\frac{f_{\Theta u}}{\tau} + \frac{f_{u\Theta}}{\tau_\Theta}\right)\langle u_i t\rangle - \left(\frac{1}{\tau} + \frac{1}{\tau_\Theta}\right)\langle\theta_L u_{Lj}\rangle}_{IV}. \qquad (6)$$

In system (6), convective transport of fluctuations and temperature (I), diffusion (II), production of fluctuations from gradients of dispersed phase average motion and temperature (III), and the interaction between the phases (IV) are taken into account.

The heat and mass transfer model for the evaporation of single droplet was described in detail [34].

4. Numerical realization and boundary conditions

4.1. Numerical realization

The numerical solution was obtained using the finite-volume method by Patankar [36]. For convective terms, the QUICK procedure was applied [37]. The diffusion fluxes were written using central differences. The pressure field was corrected by the finite-volume SIMPLEC procedure [38].

A computation non-uniform staggered grid was used. Densening of mesh nodes was applied in the recirculation zone, in the flow detachment region, and in the reattachment zone. All computations were performed on the basic grid that comprised 350×120 control volumes. Additionally, a series of test computations for a gas–droplet flow with droplet evaporation containing 400×240 CVs was performed (not shown). Nusselt numbers obtained in different computation runs differed within 1% for the single-phase flow and within 3% for the gas–droplet flow with evaporating droplets. The Nusselt number being rather sensitive to variation of mean-flow quantities and to the temperature of the two-phase flow, in the majority of computations a grid comprising 350×120 control volumes was used.

In calculating the two-phase jet flow initial conditions were set at the pipe inlet, either in the form of uniform profiles of phase parameters or in the form of distributions obtained in preliminary calculations of two-phase pipe flow. At the pipe outlet, boundary conditions consisted in setting zero derivatives of variable quantities in the longitudinal direction. At the pipe axis, for both phases conditions of symmetry were adopted. At the wall, the wall impermeability condition and the no-slip condition for the gaseous phase were used. For the dispersed phase boundary conditions were adopted [29]. After precipitation at the channel wall, droplets were assumed to stick to the surface and never return to the flow.

5. Testing for the one-phase separation air flow

At the first stage we have made a comparison with experimental data on Nusselt number distribution for one-phase turbulent flows behind sudden pipe expansion. Comparison results are presented in Fig. 2, where Nu_{fd} is Nusselt number for one-phase developed flow at other parameters being equal. Calculations and experiments have been carried out at approximately equal Reynolds number and variable step height. It is apparent that with the growth of correlation R_1/R_2 heat transfer intensity decreases in the detached area, at this, far from detachment section heat transfer increases with the growth of R_1/R_2. At that, note present secondary vortex placed near the back wall of the ledge. Indirect proof of its presence is local minimum in Nusselt number distribution at the distance $x/H \approx 1$, which concords with the data [8,11,12].

In addition, comparison with the measurement data on detached zone length for the case of friction after sudden pipe expansion [10,13] and behind the backward-facing step [31] has been carried out. This data is given in Table 1.

A good agreement was found to exist between the measured and predicted data sets, this agreement serving a basis for subsequent computations of two-phase flows.

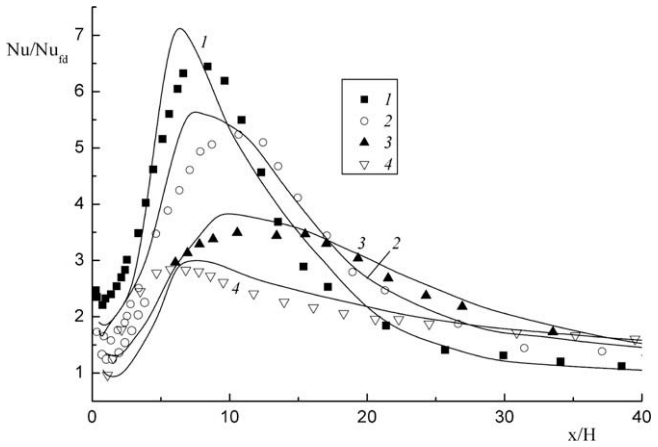

Fig. 2. Heat transfer intensification ratio downstream of the sudden pipe expansion. Symbols are experimental results of Baughn et al. [11]. *1* – $R_1/R_2 = 0.27$, $H = 35$ mm, Re = 16700; *2* – $R_1/R_2 = 0.42$, 29 mm, 17700; *3* – $R_1/R_2 = 0.53$, 22 mm, 19400; *4* – $R_1/R_2 = 0.8$, 10 mm, 20100.

Table 1
Comparison of flow reattachment length for single-phase flow.

Source	D_2/D_1 or h/H	$\mathrm{Re} \times 10^4$	x_R/H	
			Measured	Predicted
[10]	1.6	1.56	10	10.4
[13]	2.7	8.4	8.3	8.5
[31]	1.25	2.8	6.6	6.8
[21]	1.5	1.8	7.4	7.6

6. Numerical computations and its discussions

All calculations were carried out for a monodispersed gas–droplet mixture. The diameter of small tube before expansion $2R_1 = 20$ mm, behind expansion it was $2R_2 = 60$ mm, the expansion ratio was $ER = (R_2/R_1)^2 = 9$, and the step height was $H = 20$ mm. The gas flow velocity before detachment was $U_1 = 10$ m/s, Reynolds number for the gas phase was $\mathrm{Re}_H = HU_1/\nu = 13300$. The initial velocity of the dispersed phase was $U_{L1} = 0.8U_1$. The initial droplet sized varied within $d_1 = 0$–100 μm, and their mass concentration changed within $M_{L1} = 0$–0.1. The length of calculation region after the tube expansion was $30H$. The density of heat flux fed to the tube surface was $q_W = 0.5$–2 kW/m^2.

6.1. Flow structure

The profiles of axial velocity, turbulent kinetic energy, temperature of the gas phase and droplets diameter are shown in Fig. 3. Initial velocity is distributed uniformly in the inlet cross-section before flow detachment (line *1*). Curves *2–4* correspond to the zone of recirculation, and curves *5* and *6* correspond to the zone of two-phase flow development after attachment. We should note that a drastic change in the flow structure is observed downward from the detachment cross-section. For the gas velocity profiles there are areas of negative velocities, corresponding to the zone of flow recirculation.

Maximum value of gas turbulence energy can be observed in the shear layer (see Fig. 3b). Moving down the flow maximum value of turbulence energy decreases and its profile becomes more plane.

The profiles of dimensionless temperature of the gas phase $\Theta = (T - T_W)/(T_1 - T_W)$ are shown in Fig. 3c, where T_1 and T_W are the initial temperature of the flow in the detachment cross-section and the wall temperature. The uniform temperature profile is set at the inlet (line *1*). While moving downward the flow the profile of gas temperature changes (curves *2–6*). In initial cross-sections (curves *2*–3) in the axial zone temperature $\Phi < 1$, what is explained by local gas cooling because of adiabatic evaporation of droplets. Analogous results have been obtained in measurements and calculations [34] in the studies of wall mist screens. The temperature profiles directly after flow detachment ($x/H = 2$) testify an increased in thickness of the thermal mixing layer behind a backward-facing step. Intensive turbulent mixing in the detachment area leads to the fact that the most part of temperature difference is within a thin wall layer (whose thickness is about 3–5% of tube radius). Correspondingly, the value of heat transfer of the two-phase flow with the tube surface is determined by intensity of turbulent mixing of gaseous phase in the wall layer.

Fig. 3d demonstrates calculation results for the changed drop size. Note that droplets for the case $\mathrm{Stk} < 1$ exist over the whole pipe section. Drop diameter decreases both along the pipe length and its section for the account of evaporation processes, at that, in axial zone of the pipe are much larger particles than near the wall and in the area of flow recirculation.

The radial profiles of the dispersed phase mass loading ratio and mass flux at different locations over the pipe length are shown in Fig. 4 for various initial particle diameters, $d_1 = 10$ μm, $\mathrm{Stk} = 0.03$ (Fig. 4a), $d_1 = 50$ μm, $\mathrm{Stk} = 0.7$ (Fig. 4b), and $d_1 = 100$ μm, $\mathrm{Stk} = 2.7$ (Fig. 4c). It should be noted that entrains fine dispersed droplets into the separated flow readily, which are present in the stream throughout the whole pipe cross-section, whereas large particles, due to their inertia, almost never enter the recirculation region, being present only in the shear layer region (curves *2–4*). Behind the detachment point the mass fraction of fine droplets decreases sharply because of intense evaporation of particles and due to the sudden expansion of the flow field. In the wall zone, owing to evaporation the mass concentration of droplets is much lower than in the axial zone of the cylindrical channel.

Distribution of wall shear stress coefficient $C_f = 2\tau_W^2/U_1^2$ behind the detachment point is shown in Fig. 5 depending on the drop size value. It is apparent that added disperse phase has no significant impact on the value C_f both in the area of flow detachment and after reattachment point. Note there is only insignificant growth of wall shear stress in the two-phase flow. The same is valid for the one-phase flow [1], $C_f = 0$ in the area of reattachment point.

6.2. Heat transfer characteristics

Figs. 6 and 7 show the distributions of Nusselt number over the pipe length for various droplets initial diameter (Fig. 6) and its mass fraction (Fig. 7). The Nusselt numbers were calculated by the formula

$$Nu = \frac{q_W H}{\lambda(T_W - T_m)},$$

where $T_m = \frac{2}{U_1 R_2^2}\int_0^{R_2} TUrdr$ is the mean gas-flow temperature. Droplets added to the air flow substantial (more than twofold) enhance the heat transfer in comparison with the single-phase air flow (curve *1*), all other conditions being identical. Augmented heat transfer is observed both in the recirculation zone and in the relaxation region. The latter is confirmed by data in Fig. 4 showing that droplets readily become entrained with the separated flow. Fine droplets evaporate faster (over a shorter pipe length, see curve *2*) due to larger interphase surface. As more and more evaporating droplets disappear from the flow, the heat transfer rate tends to the value observed in the single-phase flow. Increased particle size acts to suppress the entrainment of particles with the recirculation flow because of increased Stokes number. For 100-μm diameter

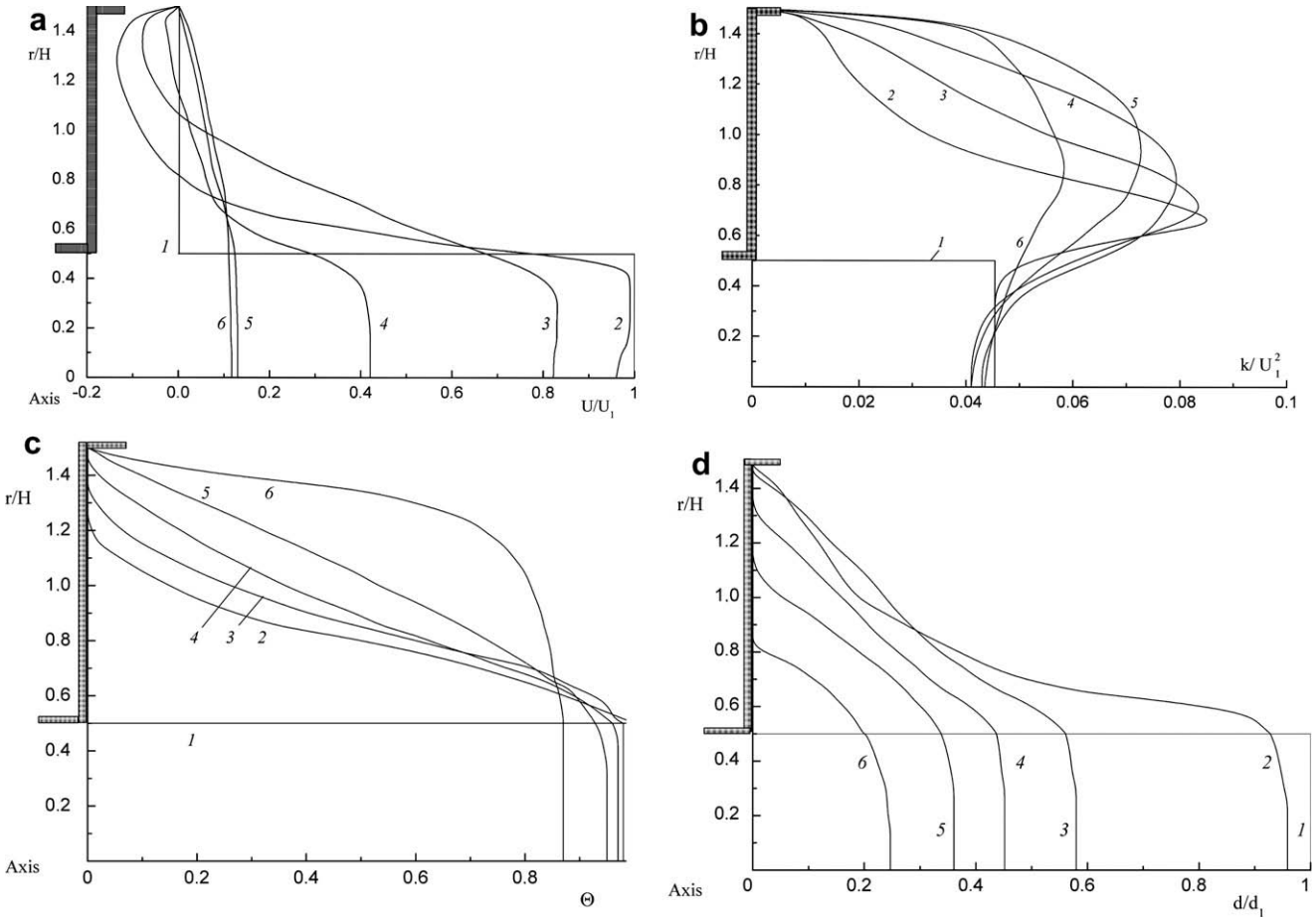

Fig. 3. Predicted profiles velocity (a), turbulent kinetic energy (b), temperature (c) of the gas phase and droplets diameter (d). d_1 = 50 μm, M_{L1} = 0.05. *1* – x/H = 0, *2* – 2, *3* – 6, *4* – 10, *5* – 15, *6* – 20.

droplets (curve *4*) the Stokes number is Stk = 2.5, the entrainment of the dispersed phase with the detached flow being therefore less pronounced. As a result, in the detachment zone the rate of heat transfer is roughly the same as in the one-phase flow; behind the reattachment point the heat transfer intensity increases due to droplet evaporation. It should be noted that under conditions with evaporation the Nusselt number in the flow laden with large droplets (d_1 = 100 μm) is smaller than the same number for finer droplets (d_1 = 50 μm) over the entire calculated flow domain.

Figs. 6 and 7(a) show the position of the reattachment point (arrows). The one-phase flow reattaches to the wall at the distance $x_R \approx 10.6H$ from the sudden expansion plane. In the case of two-phase flow the reattachment zone is more extended (see Tables 2 and 3, in which calculated reattachment lengths for gas–droplets flow are summarized). This conclusion disagrees with data previously reported by Founti et al. [19,20], who found the reattachment zone in the case of two-phase flow to be shorter than in the one-phase flow yet becoming more extended in the downstream direction with increasing concentration of liquid droplets. Note also that, in our calculations, with increasing droplet concentration the recirculation zone also became more extended, which result qualitatively complies with the data reported by Hishida et al. [17].

Distribution of the maximal Nusselt number depending on the Reynolds number, plotted by the step height and initial velocity of the gas phase, is shown in Figs. 6 and 7(b). The empirical correlation [12] was used for comparison at the single-phase flow. This correlation describes well the results obtained for the flow with axiasymmetric sudden expansion in a tube under the boundary conditions T_W = const and q_W = const,

$$\mathrm{Nu}_{max} = 0.2\mathrm{Re}_{R1}^{2/3}, \tag{7}$$

where $\mathrm{Nu}_{max} = \alpha_{max} 2R_2/\lambda$ is the maximal Nusselt number, plotted by the tube diameter after the flow expansion. For the single-phase flow after an abrupt expansion, the results of calculations by this model (line *1*) correlate satisfactory with dependence Eq. (7). With increase of Re number the maxima Nusselt number increases, what is typical both for the single-phase flow and the gas–droplets flow. For the gas–droplet flow the values of heat transfer coefficients are higher than the corresponding values, obtained for the single-phase flow (curves *2–4*) because of evaporation of the dispersed phase. The increase in the particle size decreases heat transfer because of a significant reduction of the contact interface, what is obvious in the range of low Re numbers.

Effect of disperse phase on the value of maximum heat transfer is shown in Fig. 8. Note present pronounced maximum in the distribution Nu_{max} in all studied in the work changed diapason of mass fraction of droplets. It is observed in the area of small sizes of the particles (Stk = 0.02–0.05) and conditioned by effecting factors different in their nature – more intense evaporation of droplets with small diameters, decreased velocity of their inertial deposition and weakened entrainment of larger particles in the detached flow. However, the issue requires more detailed studies. Growing concentration of disperse phase results in significant growth of heat transfer between two-phase flow and the wall compare with the one-phase flow (Stk = 0). Note that the largest increase of heat transfer is related to the area of small size of the particles getting into recirculation zone and at fixed fraction value of the droplets their number is the largest.

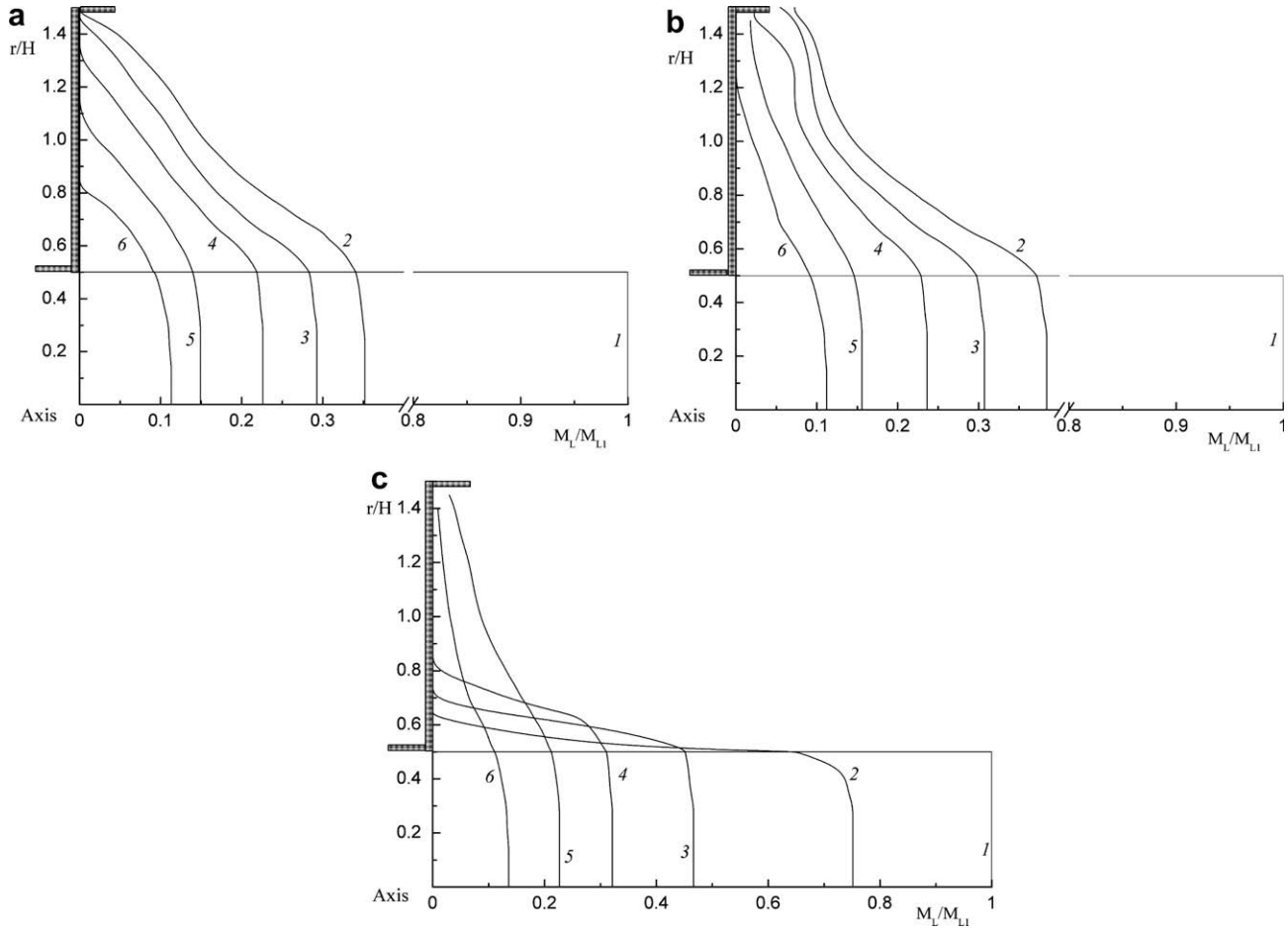

Fig. 4. Profiles of droplets mass loading ratio. $M_{L1} = 0.05$. (a) $d_1 = 10$ μm; (b) 50 μm, 0.7; (c) 100 μm. *1* – $x/H = 0$, *2* – 2, *3* – 6, *4* – 10, *5* – 15, *6* – 20.

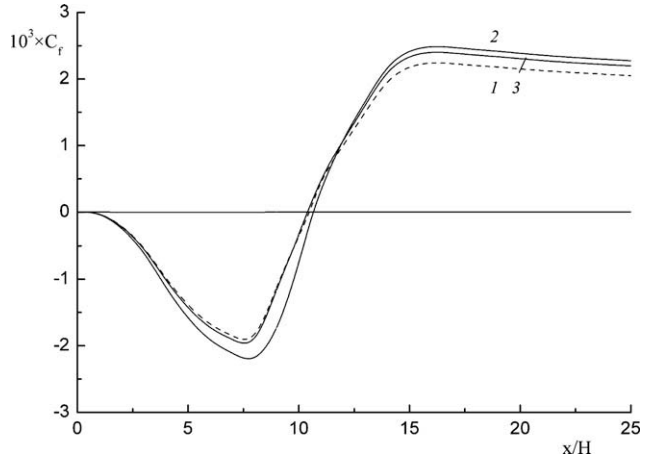

Fig. 5. Skin friction coefficient distribution along the pipe length. $H = 20$ mm, $U_{L1} = 0.8U_1$, Re = 13300, $M_{L1} = 0.05$. $q_W = 1$ kW/m^2. *1* – one-phase flow, *2* – $d_1 = 10$ μm, *3* – 100.

Fig. 9 demonstrates data on the heat flux value effecting heat transfer in the detached gas–drop flow. Dotted lines in the figure show data on heat transfer in one-phase flow at $q_W = 1$ kW/m^2. As it is shown in many works, for instance in [8,11,12,31], change of the heat flow value practically has no impact on the heat transfer coefficient. In two-phase gas–drop flow with the growing density of heat flux on the wall heat transfer intensity droplets. At minimum value of the heat flux Nusselt number increases more than 2 times compare with the one-phase flow. At that, increased heat transfer is observed over the whole length of the calculated area. Further down the flow as disperse phase evaporates Nusselt number profile coincides with the one for the single-phase air flow.

7. Comparison with experimental results for turbulent mist separated flows

Below are given comparison data only for the separated mist flow behind the plane backward-facing step. In the publications there is no data on heat and mass transfer for gas–droplets flow downstream of the sudden pipe expansion. Despite that all predictions have been carried out only for the flow after sudden pipe expansion, the below presented comparison results are useful since the detached flow behind the backward-facing step is qualitatively similar to the flow after sudden pipe expansion.

The distributions of longitudinal gas and droplet velocities over the separation length of the flow are shown in Fig. 10 for a backward-facing step of height $H = 20$ mm. The experiment was performed by Hishida et al. [17]. The our calculations were carried out for the following initial conditions: downward flow; developed flow upstream of the flow detachment point; back-facing step of height $H = 20$ mm; channel expansion ratio $ER = R_1/R_2 = 1.14$; the mean-flow velocity in cross-section before separation $U_1 = 10$ m/s; $Re_H = U_1 H/\nu = 11000$; mass concentration of water droplets $M_{L1} = 4\%$; density of water droplets $\rho_L = 1000$ kg/m^3; initial droplet size $d_1 = 60$ μm; wall temperatures $T_W = 308$, 323 and 338 K; flow

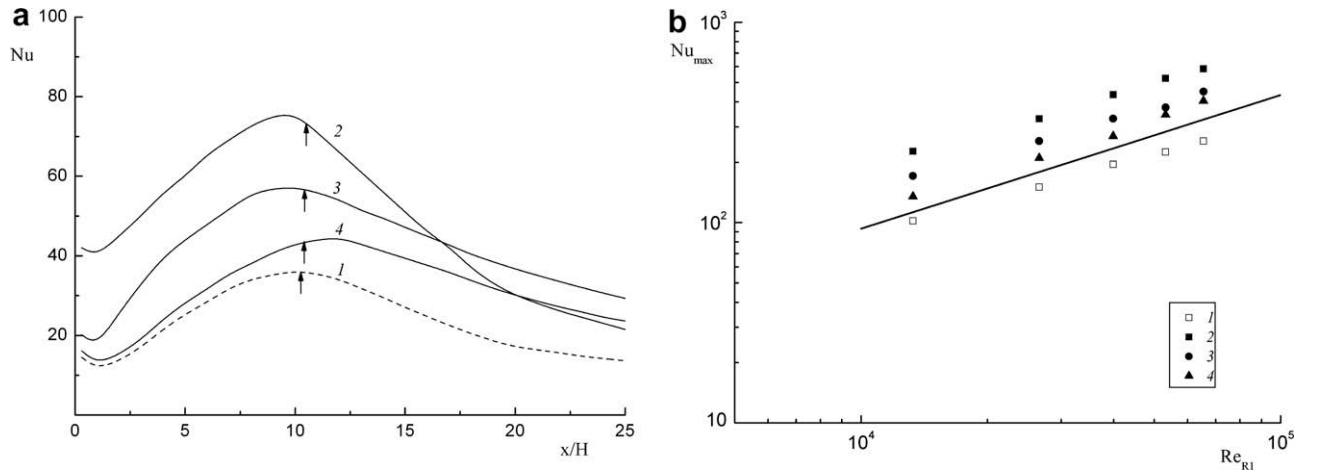

Fig. 6. Predicted local Nusselt number distribution along the pipe length (a) and maximum Nusselt number as a function of Reynolds number. $M_{L1} = 0.05$. Solid line is the correlation Baughn et al. [12]. *1* – one-phase flow, *2* – $d_1 = 10$ μm; *3* – 50, *4* – 100.

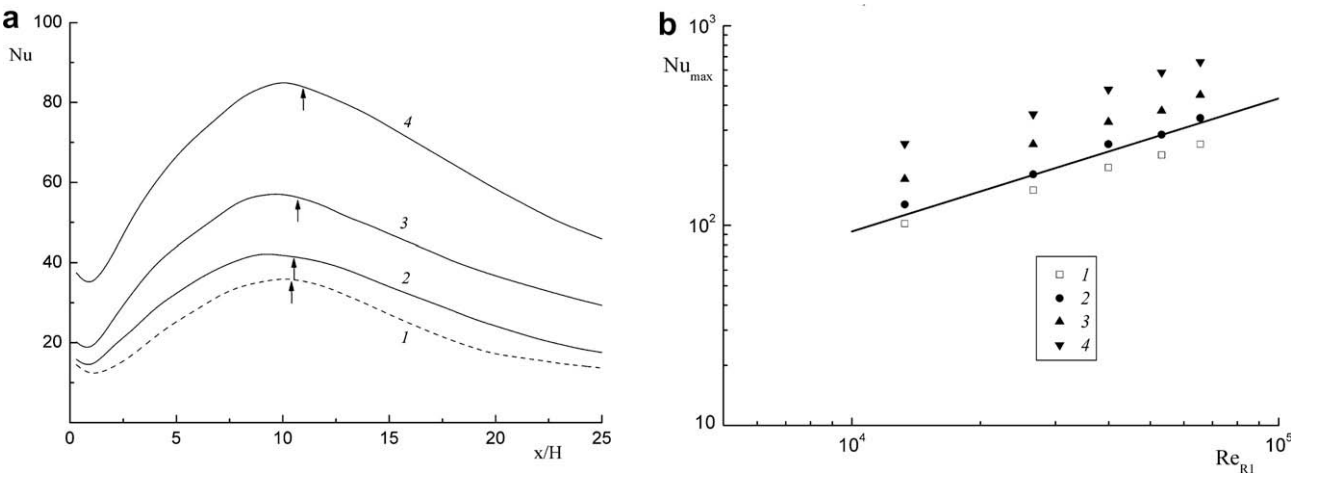

Fig. 7. Local Nusselt number distribution along the pipe length (a) and maximum Nusselt number as a function of Reynolds number. $d_1 = 50$ μm. Solid line is the correlation Baughn et al. [12]. *1* – one-phase flow, *2* – $M_{L1} = 0.02$; *3* – 0.05; *4* – 0.1.

Table 2
Length of separated flow region of gas–droplets flow after sudden pipe expansion depending on droplets concentration $d_1 = 50$ μm.

M_{L1}	0	0.01	0.02	0.05	0.07	0.1
X_R/H	10.6	10.6	10.8	10.9	11	11.1

Table 3
Reattachment length for gas–droplets flow downstream of sudden pipe expansion at variable size of disperse phase $M_{L1} = 0.05$.

d_1 (μm)	0	10	50	100
X_R/H	10.6	10.75	10.9	10.95

temperature $T_1 = 293$ K. The comparative data show that the gas-phase velocity behaves similarly to the case of one-phase flow. It should be noted that immediately behind the step there forms a zone free of the dispersed phase. Owing to inertia, droplets do not enter the recirculation flow region and move only in the shear layer. The mean-flow Stokes number, which characterizes the degree to which the dispersed phase is involved in the turbulent motion of the carrier medium for the case of a 20-mm step is $\mathrm{Stk} = \tau/\tau_f \approx 1.1$. The particle velocity is greater than the gas velocity also owing to droplet inertia.

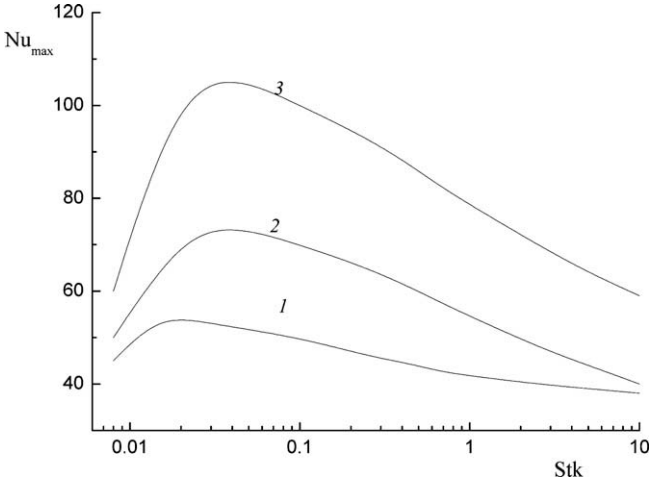

Fig. 8. The effect of the Stokes number on the distribution of the maximum heat transfer number. *1* – $M_{L1} = 0.02$, *2* – 0.05, *3* – 0.1.

The effect due to added droplets on heat transfer is illustrated by Fig. 11 for two step heights, 10 mm (see Fig. 11a) and 20 mm

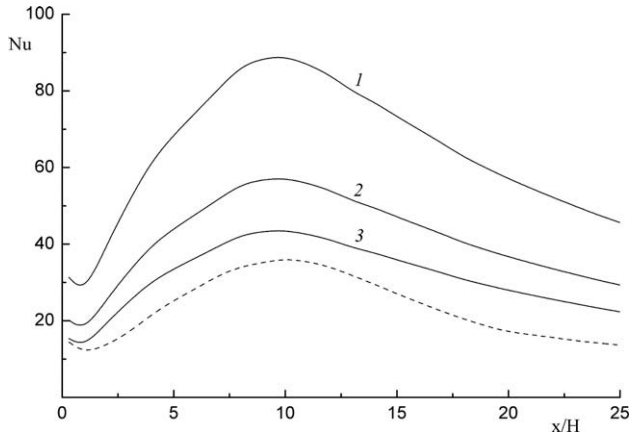

Fig. 9. Enhancement of Nusselt number changing heat flux density. $M_{L1} = 0.05$, $d_1 = 50$ μm. *1* – $q_W = 0.5$ kWt/m^2; *2* – 1; *3* – 2.

(see Fig. 11b). Here, $St_{0,max}$ is the maxima Stanton number for the one-phase air flow, and x_R is the coordinate of the flow reattachment point. The Stanton number was calculated by the formula $St = \alpha/(\rho C_P U_1)$; here, α is the heat transfer coefficient and U_1 is the flow velocity. An analysis of the data in Fig. 12 shows that the rate of heat transfer in the case of gas–droplet flow increases appreciably (more than 50%) for steps of both heights. An increase in the wall temperature leads to a reduction of the heat transfer intensity. It is agreed with our measurements and numerical predictions [34]. For the most part, heat transfer intensification ratio is observed in the region behind the flow reattachment point, that indicative of a small number of droplets entering the recirculation region. Note that for the case $H = 10$ mm the value $St/St_{0,max}$ is higher in the area of flow renewal that in the case with the step with 20 mm high. In the detached area heat transfer in case of the step $H = 20$ mm (Stk = 1.1) high is higher than for the case with the step of $H = 10$ mm (Stk = 2.2) because of the fact that at lesser Stokes number droplets are better entrained into recirculation flow. In Fig. 11a maximum heat transfer is far behind the reattachment point ($\frac{x-x_R}{x_R} \approx 2-4$), that can be explained by bad entrainment of the particles into the detached flow at large Stokes numbers. At that, from Fig. 11b it is apparent that maximum heat transfer approximately coincides with the reattachment point.

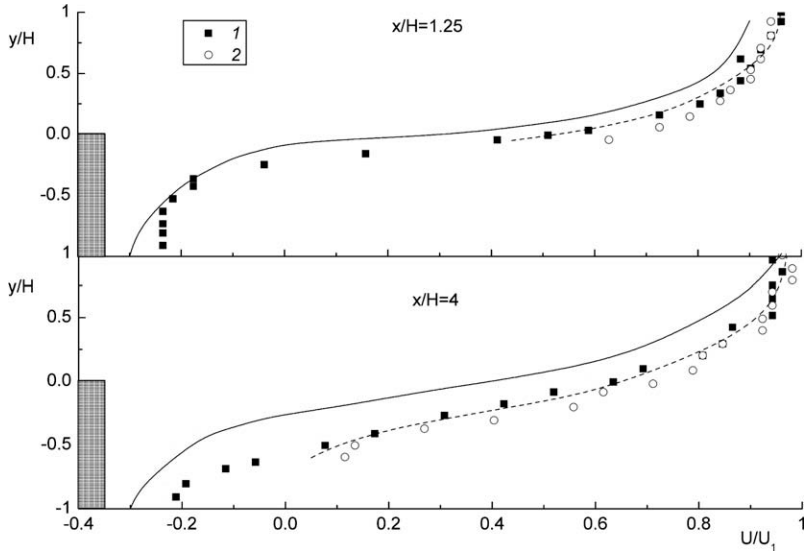

Fig. 10. Gas (solid curves) and droplets (dashed curves) mean velocity profiles in backward-facing step flow. Symbols are measurements of [17]: *1* – gas, *2* – droplets, curves are predictions of the work.

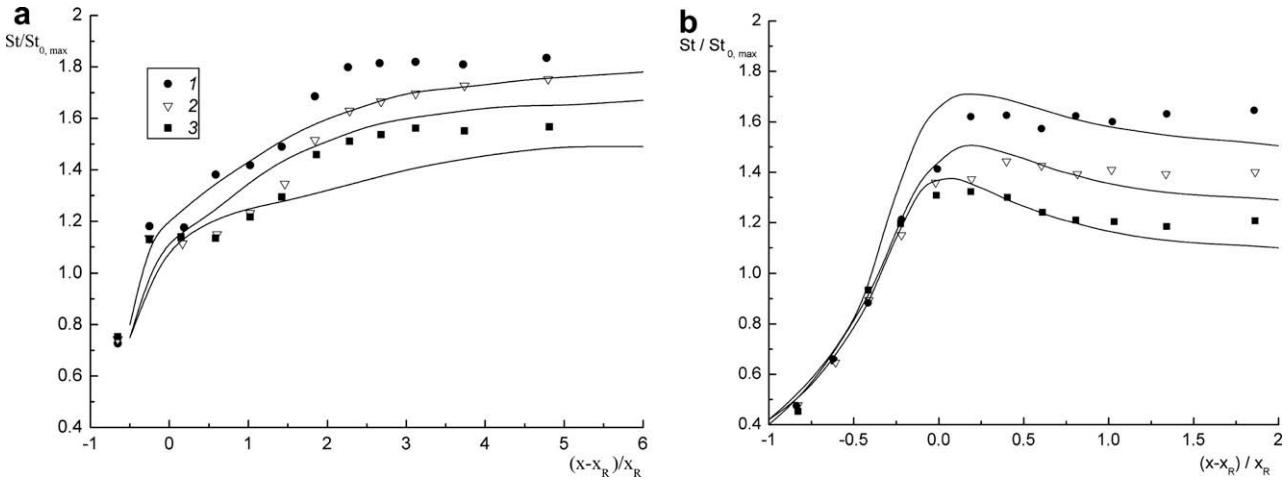

Fig. 11. Heat transfer enhancement in gas–droplets flow behind the backward-facing flow. Symbols are experimental results by Hishida et al. [17], curves are computations of the present paper. (a) $H = 10$ mm, (b) $H = 20$ mm. *1* – $T_W = 338$ K, *2* – 323 K, *3* – 308 K.

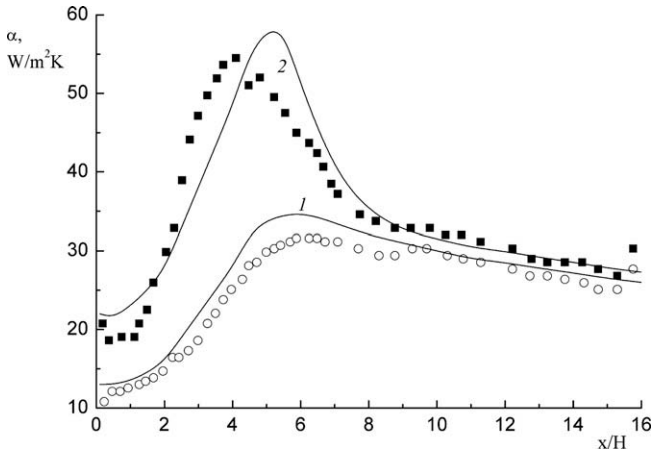

Fig. 12. Heat transfer coefficient distributions in two-phase flow behind the backward-facing flow. Symbols are experiments of [25], curves are the calculations of the work. *1* – $M_{L1} = 0$, *2* – 0.015%.

Since a small amount of finely dispersed droplets added to the flow cannot substantially modify the gas phase turbulence, the heat transfer augmentation in gas–droplet flows should be attributed to the use of the phase change heat due to droplet evaporation in the wall region.

Comparison on heat transfer in mist flow with low mass fraction of droplets [25] are demonstrated in Fig. 12. The amount of mist used here was about 0.015% as a mass ratio to the amount of the main air flow. The diameter of mist water droplets was about 10 μm. A fully developed temperature field was obtained by the heated plate downstream the entrance of channel expanded. The entrance section height was $h_1 = 60$ mm, backward-facing step height $H = 40$ mm, the channel expand ratio $ER = 1.67$. Reynolds number is $\mathrm{Re} = U_1 H/\nu = 12500$ and main flow velocity $U_1 = 5$ m/s. Experiments carried out in heat flux $q_W = 176$ W/m^2. Spray was blown out of the small hole situated in the upper part of the step.

In the local heat transfer distribution, the maximum heat transfer coefficient located at $x/H \approx 6$ without mist. The heat transfer coefficient distributions upstream the reattachment point shows lower values because of forming the recirculation zone witch was surrounded the shear layer of the separating flow and duct wall. On the other hand, with respect to be induced mist to the main flow, the maximum heat transfer coefficients α_{max} was obtained in experiments at $x/H \approx 4.5$, which was shorter than that in our computations. The heat transfer rate considerably increased both in the recirculation and the reattachment regions compared with no-mist conditions. It is seen that the local heat transfer distributions upstream the maximum point especially increase, due to decrease the temperature in the gas stream. The heat transfer was enhanced by air flow contained the mist of even fine and small quantity of liquid water droplets. This is specific both for the measurements [25] and our calculations.

8. Conclusions

Fine droplets (with a small Stokes number) get readily entrained with the detached flow, spread throughout the whole pipe cross-section. On the contrary, large particles, due to their inertia, avoid trapping in the recirculation zone, being therefore present only in the shear layer region. In the wall zone, due to droplet evaporation, the concentration of liquid droplets is much lower than in the axial region of the cylindrical channel. Addition of liquid particles to the flow results in a pronounced (twofold) heat transfer intensification in comparison with the single-phase air flow, all other conditions being identical. Here, intensification of heat transfer both in the recirculation zone and in the flow development region in the case of fine particles (Stokes number $\mathrm{Stk} < 0.7$) is noteworthy. The latter observation lends support to the conclusion that finely dispersed particles get entrained with the detached flow. Relatively large particles ($\mathrm{Stk} = 2.7$) added to the flow almost never enter the recirculation zone, the heat transfer intensity in this zone remains roughly unchanged, and enhanced heat transfer is only observed in the reattachment zone.

An increase in the initial droplet diameter decreases the Nusselt number due to interphase contact area reduction at fixed mass concentration of droplets.

Results of a comparative analysis with previously reported experimental and numerical data for sudden expansion two-phase flows through round pipes and for plane flows past a backward-facing step are presented.

This work was partially supported by the Russian Foundation for Basic Research (Projects No. 09-08-00929).

Acknowledgements

Authors thanks Dr. N.I. Yarygina (IT SB RAS, Novosibirsk, Russia), Dr. M. Founti (National Technical University of Athens, Athens, Greece), Prof. Y. Hardalupas (Imperial College, London, UK) and Prof. L.I. Zaichik (Nuclear Safety Institute RAS, Moscow, Russia), for stimulating discussions.

References

[1] P.K. Chang, Separation of Flow, Pergamon Press, Oxford, 1970.
[2] J.K. Eaton, J.P. Johnston, Review of research on subsonic turbulent flow reattachment, AIAA J. 19 (1981) 1093–1100.
[3] V.E. Alemasov, G.A. Glebov, A.P. Kozlov, Methods of Thermoanemometer Study of Separation Flow, Publ. House of Kazan Branch of Academy of Sciences of USSR, Kazan, 1989 (in Russian).
[4] R.L. Simpson, Aspects of turbulent boundary-layer separation, Prog. Aerospace Sci. 32 (1996) 457–521.
[5] T. Ota, A survey of heat transfer in separated and reattached flows, Appl. Mech. Rev. 53 (2000) 219–235.
[6] R. Ruderich, H. Fernholz, An experimental investigation of a turbulent shear flow with separation, reverse flow and reattachment, J. Fluid Mech. 163 (1986) 283–322.
[7] I.P. Castro, A. Hague, The structure of a turbulent shear layer bounding a separation region, J. Fluid Mech. 179 (1987) 439–468.
[8] A.F. Polyakov, P.L. Komarov, Study of characteristics of turbulence and heat transfer behind a backward-facing step in a slot channel, Preprint of Institute of High Temperature of RAS, 1996, 70 p. (in Russian).
[9] H. Le, P. Moin, J. Kim, Direct numerical simulation of turbulent flow over a backward-facing step, J. Fluid Mech. 330 (1997) 349–374.
[10] M. Stieglmeier, C. Tropea, N. Weiser, W. Nitsche, Experimental investigation of the flow through axisymmeric expansions, Trans. ASME J. Fluid Eng. 111 (1989) 464–471.
[11] J.W. Baughn, M.A. Hoffman, R.K. Takahasi, B.E. Lounder, Local heat transfer downstream of an abrupt expansion in a circular channel with constant wall heat flux, Trans. ASME J. Heat Transfer 106 (1984) 789–796.
[12] J.W. Baughn, M.A. Hoffman, B.E. Lounder, D. Lee, C. Yap, Heat transfer, temperature, and velocity measurements downstream of an abrupt expansion in a circular tube at uniform wall temperature, Trans. ASME J. Heat Transfer 111 (1989) 870–877.
[13] R.P. Durrett, W.H. Stevenson, H.D. Thompson, Radial and axial turbulent flow measurements with an LDV in an axisymmeric sudden expansion air flow, Trans. ASME J. Fluid Eng. 110 (1988) 367–372.
[14] B. Ruck, B. Makiola, Particle dispersion in a single-sided backward-facing step flow, Int. J. Multiphase Flow 14 (1988) 787–800.
[15] Y. Hardalupas, A.M.K.P. Taylor, J.H. Whitelaw, Particle dispersion in a vertical round sudden-expansion flow, Phil. Trans. Roy. Soc. Lond. A 341 (1992) 411–442.
[16] L.I. Zaichik, M.V. Kozelev, V.A. Pershukov, Prediction of turbulent gas-dispersed channel flow with recirculation zones, Fluid Dyn. 29 (1994) 65–75.
[17] K. Hishida, T. Nagayasu, M. Maeda, Augmentation of convective heat transfer by an effective utilization of droplet inertia, Int. J. Heat Mass Transfer 38 (1995) 1773–1785.
[18] L.I. Zaichik, V.A. Pershukov, M.V. Kozelev, A.A. Vinberg, Modeling of dynamics, heat transfer, and combustion in two-phase turbulent flow: 1. Isothermal flow, Exp. Thermal Fluid Sci. 15 (1997) 291–310.
[19] T. Achimastos, D. Dimopoulos, A. Klipfel, M. Founti, Measurements and predictions in a vertical sudden expansion two-phase flow: the effects of

particle concentration, Proc. 7th Int. Workshop Two-Phase Flow Predictions. Erlangen, Germany, 1994.
[20] M. Founti, A. Klipfel, Experimental and computational instigations of nearly dense two-phase sudden expansion flows, Exp. Thermal Fluid Sci. 17 (1998) 27–36.
[21] J.R. Fessler, J.K. Eaton, Turbulence modification by particles in a backward-facing step flow, J. Fluid Mech. 314 (1999) 97–117.
[22] H.Q. Zhang, C.K. Chan, K.S. Lau, Numerical simulation of sudden-expansion particle-laden flows using an improved stochastic separated flow model, Int. J. Numerical Heat Transfer A 40 (2001) 89–102.
[23] K.F. Yua, K.S. Lau, C.K. Chan, Numerical simulation of gas-particle flow in a single-side backward-facing step flow, J. Comp. Appl. Math. 163 (2004) 319–331.
[24] M. Pakhomov, V. Terekhov, Heat and mass transfer in gas–drops turbulent flow with separation and evaporation, Proc. ICHMT Int. Symp. Advances Computational Heat Transfer CHT-08, Marrakech, Morocco, May 11–16, 2008, CD-disc, Paper 151, 20 p.
[25] Y. Miyafuji, I. Senaha, K. Oyakawa, M. Hiwada, Enhancement of heat transfer at downstream of a backward-facing step by mist flow, Proc. 2nd Int. Conf. Jets, Wakes and Separated Flows ICJWSF-2008, September 16–19, 2008, TU of Berlin, Berlin, Germany, CD-disc, 7 p.
[26] K. Mastanaiah, E.N. Ganic, Heat transfer in two-component dispersed flow, Trans. ASME J. Heat Transfer 103 (1981) 300–306.
[27] I.V. Derevich, L.I. Zaichik, Particle deposition from a turbulent flow, Fluid Dyn. 23 (1988) 722–729.
[28] R. Clift, J.R. Grace, M.E. Weber, Bubbles, Drops and Particles, Academic Press, New York, 1978.
[29] I.V. Derevich, The hydrodynamics and heat transfer and mass transfer of particles under conditions of turbulent flow of gas suspension in a pipe and in an axisymmetric jet, High Temp. 40 (2002) 78–91.
[30] C.B. Hwang, C.A. Lin, Improved low-Reynolds-number k–$\tilde{\varepsilon}$ model based on direct simulation data, AIAA J. 36 (1988) 38–43.
[31] J.C. Vogel, J.K. Eaton, Combined heat transfer and fluid dynamics measurements downstream of a backward-facing step, Trans. ASME J. Heat Transfer 107 (1985) 922–929.
[32] J.L. Lumley, The second order model for turbulent flows, in: Prediction Methods for Turbulent Flow, Hemisphere, New York.
[33] T.B. Gatski, C.G. Speziale, On explicit algebraic stress models for complex turbulent flows, J. Fluid Mech. 254 (1993) 59–78.
[34] V.I. Terekhov, M.A. Pakhomov, The thermal efficiency of near-wall gas–droplets screens. I. Numerical modeling, Int. J. Heat Mass Transfer 48 (2005) 1747–1759.
[35] O. Simonin, Prediction of the dispersed phase turbulence in particle-laden jet, Proc. 1st ASME-JSME Fluid Eng. Conf., Portland, OR, USA, June 23–27, 1991, pp. 197–206.
[36] S.V. Patankar, Numerical Heat Transfer and Fluid Flow, Hemisphere, New York, 1980.
[37] B.P. Leonard, A stable and accurate convective modelling procedure based on quadratic upstream interpolation, Comput. Methods Appl. Mech. Eng. 19 (1979) 59–79.
[38] J.P. Van Doormaal, G.D. Raithby, Enhancements of the SIMPLE method for predicting incompressible fluid flow, Int. J. Numer. Heat Transfer A 7 (1984) 147–164.